Direct Torque and Predictive Control Strategies in Nine-phase Electric Drives Using Virtual Voltage Vectors

Paula G. Entrambasaguas, Ivan Zoric, Ignacio Gonzalez-Prieto, Mario J. Duran and Emil Levi, *Fellow, IEEE*

***Abstract* – One of the main distinctive features of multiphase machines is the appearance of new degrees of freedom (x-y voltages/currents) that do not exist in their three-phase counterparts. As a direct consequence, control approaches that apply a single switching state during the sampling period cannot achieve zero average x-y voltage production. In direct torque control (DTC) this implies that x-y currents are not regulated, whereas in finite-control-set model predictive control (FCS-MPC) an enhanced x-y current regulation is feasible only at the expense of disturbing the flux/torque production. Aiming to avoid these shortcomings, this work makes use of the concept of synthetic/virtual voltage vectors (VVs) to nullify/limit the x-y voltage production in order to improve the current regulation in the secondary planes. Two strategies using two and four virtual voltage vectors (2-VV and 4-VV, respectively) are proposed and compared with the standard case that applies a single switching state. Since standard MPC has the capability to indirectly regulate x-y currents, the improvements with the inclusion of VVs are expected to be more significant in DTC strategies. Experimental results validate the proposed VVs and confirm the expectations through a detailed performance comparison of standard, 2-VV and 4-VV approaches for DTC and MPC strategies.**

***Index Terms* – *Induction machine, model predictive control, direct torque control, virtual voltage vector*.**

I. INTRODUCTION

Multiphase drives are drawing much attention in recent times both in academic and industrial circles. The additional degrees of freedom, which do not exist in conventional three-phase systems, provide them with a certain degree of fault tolerance [1]-[3]. This is an attractive feature in applications where safety is considered a critical factor, as in the case of "more-electric" aircraft, electric vehicles or electric ship propulsion [4]-[12]. While the use of the extra current components has been studied for a long time, some novel advantages of the x-y current injection have been recently explored [13]. The voltage balancing of series-connected voltage source converters (VSCs) for wind energy applications [14], the unequal power distribution in multi three-phase energy conversion systems for microgrids [15], or the use of enhanced integrated on-board battery chargers for electric vehicles [16] can be cited as some examples of the innovative uses of the x-y currents.

However, standard control techniques for three-phase systems cannot regulate x-y currents and consequently these appealing features come with a price: it becomes mandatory to design more complex control strategies that properly perform the x-y current control. When using an indirect rotor field-oriented control (IRFOC) strategy the solution is relatively straightforward. It is enough to extend the use of proportional-integral (PI) controllers to regulate the secondary currents to track their zero reference values [17]-[19]. Since FOC-based control schemes use a pulse width modulation (PWM) stage for the control action, the simultaneous regulation of fundamental and secondary planes is feasible. On the contrary, those control schemes that rely on the application of a single switching state during the whole sampling period (e.g. DTC and FCS-MPC) cannot regulate all voltage components at the same time [20].

In the case of DTC, the use of look-up tables that regulate the flux and torque fully disregard the x-y components and consequently the control of the secondary currents is simply non-existent. This typically leads to high x-y currents due to the low impedance of the x-y subspace (stator resistance and leakage inductance in distributed-winding machines). Even though the speed regulation can be satisfactorily achieved, the power quality and efficiency are dramatically reduced and the final performance is poor. The case of MPC is slightly different compared to DTC because it is possible to include a weighting factor in the cost function to take into account the x-y current production. Unfortunately, this consideration does not change the fact that a single switching state has a fixed voltage contribution in the different planes. Consequently, any attempt to minimize the x-y currents highly disturbs the dynamics of the drive and eventually leads to instability.

As a solution to this problem, the concept of virtual vectors (VVs) was introduced in [21]. The newly defined VVs, originally applicable to the DTC strategy for five-phase drives, allow the application of two voltage vectors per sampling period. The formation of the virtual vectors is done offline and the aim is to maximize the α-β currents (torque and flux producing components) and minimize the x-y currents (stator copper loss producing components). This

Manuscript received October 9, 2018; revised December 2, 2018; accepted March 16, 2019.

This work was supported by the Spanish Ministry of Science and Innovation under Project ENE2014-52536-C2-1-R.

P. G. Entrambasaguas, I. Gonzalez-Prieto and M.J. Duran are with the Department of Electrical Engineering at the University of Malaga, Spain, e-mail: paulaentrambasaguas@gmail.com, ignaciogp87@gmail.com and mjduran@uma.es

I. Zoric is with Dyson, Tetbury Hill, Malmesbury SN16 0RP Wiltshire, U.K, e-mail: ivanzoric497@gmail.com.

E. Levi is with the Faculty of Engineering and Technology, Liverpool John Moores University, Liverpool L3 3AF, U.K, e-mail: e.levi@ljmu.ac.uk.

concept has been used to control five-phase induction machines [21]-[23], six-phase induction machines [24]-[28] and six-phase permanent-magnet machines [29]-[30]. The application of VVs was subsequently also extended to MPC-based strategies for five-phase permanent-magnet and six-phase induction machines [31] - [32].

Up to now, the regulation of secondary currents when MPC and DTC strategies are used has only been achieved in systems where only one x-y subspace exists. However, in systems with a number of phases greater than six, new secondary subspaces appear and, consequently, the creation of VVs becomes more complex. Taking into account that different intrinsic applications of n-phase drives have been industrially implemented using multiple sets of three-phase windings ($n = 3k$, with $k = 3, 4, 5$ [20]), it is timely to extend the use of VVs to higher-order multiphase machines. Specifically, this work focuses on nine-phase induction motor drives with three isolated neutral points and explores the possibility to create VVs that can be used together with DTC or MPC approaches.

Aiming to make a complete analysis, the study has been structured in three unique steps that provide the following contributions:

- C1: As a first step, the use of virtual vectors based on four switching states is examined (termed 4-VV in what follows). By properly selecting the four switching states that are combined within the VV, it is possible to achieve a zero contribution in all secondary planes. It must be noted however that producing zero x-y voltages comes at the expense of a higher effective switching frequency.
- C2: As a second step, the creation of VVs from two different switching states is explored (termed 2-VV in what follows). Contrary to the 4-VV approach, the lower number of voltage vectors of 4-VV allows obtaining only a low voltage contribution in the x_1-y_1 and x_2-y_2 secondary planes. The x_1-y_1 and x_2-y_2 voltages cannot be fully nullified as in the case of six-phase drives [32].
- C3: As a final step, the 4-VV and 2-VV are used together with DTC and MPC approaches. The experimental results compare: *i)* the different performances obtained using standard and virtual voltages vectors and *ii)* the different sensitivity of DTC and MPC to the use of VVs. While it is expected that *i)* will determine the degree of improvement that can be achieved using VVs, the conclusions from *ii)* will establish whether the use of VVs is mandatory or optional for DTC and MPC.

The paper is structured as follows. In Section II the construction of 4-VV and 2-VV for a nine-phase induction machine is presented. Sections III and IV describe the VV-based MPC and DTC control strategies, respectively. Section V includes the experimental tests for standard and VV-based DTC and MPC, while the conclusions are finally summarized in Section VI.

II. VIRTUAL VOLTAGE VECTORS IN NINE-PHASE SYSTEMS

A. *Generalities of nine-phase systems*

The electric drive considered in this paper consists of an asymmetrical nine-phase induction machine with distributed windings. It is composed of three sets of three-phase windings termed $a_1b_1c_1$, $a_2b_2c_2$ and $a_3b_3c_3$, spatially shifted 20º and with three isolated neutrals. This machine is supplied by a nine-leg two-level voltage source converter (VSC) connected to a single dc-link (Fig. 1).

Even though the nine-dimensional system can be mathematically described in phase variables, a better insight can be obtained using the vector space decomposition (VSD) into orthogonal subspaces [33]. In machines with distributed windings and negligible spatial harmonics, as in this study, only the fundamental subspace (α-β) produces torque and flux, whereas the secondary components, mapped in the x_1-y_1 and x_2-y_2 subspaces, only produce additional stator copper losses. The VSD also provides the zero sequence components (z_1-z_2-z_3), but they are omitted from the analysis because the neutrals are isolated and consequently zero-sequence currents cannot flow. The VSD is performed using the generalized Clarke transformation, that in its amplitude invariant version can be expressed as:

$$[T] = \frac{2}{9}\cdot\begin{bmatrix} 1 & c(\theta) & c(2\theta) & c(6\theta) & c(7\theta) & c(8\theta) & c(12\theta) & c(13\theta) & c(14\theta) \\ 0 & s(\theta) & s(2\theta) & s(6\theta) & s(7\theta) & s(8\theta) & s(12\theta) & s(13\theta) & s(14\theta) \\ 1 & c(5\theta) & c(10\theta) & c(30\theta) & c(35\theta) & c(40\theta) & c(60\theta) & c(65\theta) & c(70\theta) \\ 0 & s(5\theta) & s(10\theta) & s(30\theta) & s(35\theta) & s(40\theta) & s(60\theta) & s(65\theta) & s(70\theta) \\ 1 & c(7\theta) & c(14\theta) & c(42\theta) & c(49\theta) & c(56\theta) & c(84\theta) & c(91\theta) & c(98\theta) \\ 0 & s(7\theta) & s(14\theta) & s(42\theta) & s(49\theta) & s(56\theta) & s(84\theta) & s(91\theta) & s(98\theta) \\ 1/3 & 0 & 0 & 1/3 & 0 & 0 & 1/3 & 0 & 0 \\ 0 & 1/3 & 0 & 0 & 1/3 & 0 & 0 & 1/3 & 0 \\ 0 & 0 & 1/3 & 0 & 0 & 1/3 & 0 & 0 & 1/3 \end{bmatrix} \quad (1)$$

$$[\alpha \;\; \beta \;\; x_1 \;\; y_1 \;\; x_2 \;\; y_2 \;\; z_1 \;\; z_2 \;\; z_3]^T = [T]\cdot[a_1 \;\; a_2 \;\; a_3 \;\; b_1 \;\; b_2 \;\; b_3 \;\; c_1 \;\; c_2 \;\; c_3]^T$$

where $\theta = \pi/9$ is the phase shift angle and c and s denote cosine and sine, respectively.

The phase voltages $[v_k]$ are obtained from the dc-link voltage V_{dc} and the switching function of the converter states $[S_k]$ as:

$$[v_k]^T = \frac{V_{dc}}{3}\begin{bmatrix} 2 & 0 & 0 & -1 & 0 & 0 & -1 & 0 & 0 \\ 0 & 2 & 0 & 0 & -1 & 0 & 0 & -1 & 0 \\ 0 & 0 & 2 & 0 & 0 & -1 & 0 & 0 & -1 \\ -1 & 0 & 0 & 2 & 0 & 0 & -1 & 0 & 0 \\ 0 & -1 & 0 & 0 & 2 & 0 & 0 & -1 & 0 \\ 0 & 0 & -1 & 0 & 0 & 2 & 0 & 0 & -1 \\ -1 & 0 & 0 & -1 & 0 & 0 & 2 & 0 & 0 \\ 0 & -1 & 0 & 0 & -1 & 0 & 0 & 2 & 0 \\ 0 & 0 & -1 & 0 & 0 & -1 & 0 & 0 & 2 \end{bmatrix}[S_k]^T \quad (2)$$

where $k = a_1, a_2, a_3, b_1, b_2, b_3, c_1, c_2, c_3$ and $S_k = 1$ if the upper switch of leg k is closed, $S_k = 0$ otherwise.

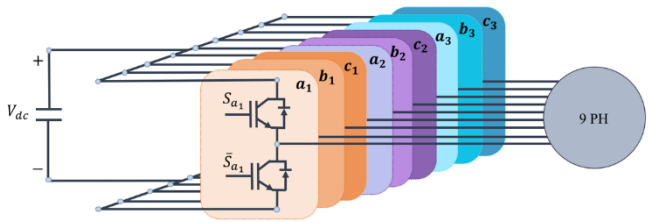

Fig. 1. Nine-phase induction machine supplied by a two-level nine-leg VSC connected to a single dc-link.

As the number of phases increases, so does the number of possible switching states of the converter. In the case of a two-level nine-phase converter, there are $2^9 = 512$ possible switching states. Making use of Clarke's transformation from (1), each of these possible switching states is mapped in all system subspaces (Fig. 2).

The aim is to maximize the α-β and to minimize the x_1-y_1 and x_2-y_2 voltage production in order to obtain desired flux and torque with minimum copper losses. However, a single switching state cannot simultaneously achieve both requirements. The best option is to select large vectors in the α-β plane (orange diamonds in Fig. 2a) because they are mapped as small vectors in the x_1-y_1 and x_2-y_2 planes (Figs. 2b-2c). Nevertheless, it can be observed that the contribution is still significant in the secondary planes and this may lead to high circulating currents when the value of the stator leakage inductance is low.

Aiming to solve this problem, recent research has suggested the use of the so-called virtual voltage vectors (VVs) [21]-[23], [28] and [31]-[32]. The main idea is to combine several switching states with such a fixed application time proportion that the average voltage production in the x-y plane(s) is zero. This procedure ideally leads to zero average x-y currents, allowing the flux and torque regulation with enhanced efficiency. Considering the six-phase system as a case example, large vectors that are aligned in the α-β plane happen to be mapped in opposite directions in the x-y plane. As a consequence, the use of only two voltage vectors per each sampling period suffices to zero the x-y voltage production with high α-β contribution [21]. A similar concept has also been used in five and six-phase machines for the MPC, [31]-[32], and DTC, [21]-[30], strategies.

While five- and six-phase systems only have one x-y plane, the nine-phase ones have at least two secondary planes (x_1-y_1 and x_2-y_2, when neutrals are isolated). Due to both the appearance of additional voltage vectors and new subspaces, the complexity of nine-phase systems becomes higher and, consequently, the concept of virtual vectors needs to be revisited.

First of all, it must be analyzed which vectors contribute most to the voltage production in the α-β plane while producing less losses in the x_1-y_1 and x_2-y_2 subspaces. This is quantified by an α-β voltage generation ratio in relation to x_1-y_1 and x_2-y_2 voltages:

$$R_{\alpha\beta} = \frac{|v_{\alpha\beta}|}{\sqrt{|v_{x_1y_1}|^2 + |v_{x_2y_2}|^2}} \tag{3}$$

where $|v_{\alpha\beta}|$, $|v_{x_1y_1}|$and $|v_{x_2y_2}|$ denote the modulus of the voltage vectors in different VSD subspaces. In order to ease the identification of switching states with the best ratio, voltage vectors have been classified in ten octadecagons labelled from O_1 to O_{10} in descending order of $|v_{\alpha\beta}|$. The amplitudes of the octadecagons in different subspaces and the α-β ratio of voltage generation are summarized in Table I.

There is no doubt that O_1 has the best conditions with regard to α-β production and minimization of x_1-y_1 and x_2-y_2 voltages, since the ratio is $R_{\alpha\beta} = 3.3$. Considering this ratio as 100%, O_2 presents the next highest α-β production, and so on. In the present study, the voltage vectors included in O_1 (orange diamonds in Fig. 2) and O_2 (red squares in Fig. 2) have been considered for the formation of virtual vectors.

B. Virtual voltage vectors using four switching states (4-VV)

It is clear from the analysis in section II.A that the use of the voltage vectors obtained by applying a single switching state cannot fulfil the requirements of the secondary planes (x_1-y_1 and x_2-y_2). Following the idea of [21], this section explores the possibility to create virtual voltage vectors (VVs) with multiple switching states in order to nullify the average voltage production in the x_1-y_1 and x_2-y_2 planes. The procedure to create the VVs involves three steps:

i) Determination of how many switching states are necessary.

While in six-phase drives there is a single x-y plane and it is sufficient to use two switching states for this purpose, it can be intuitively assumed that the nine-phase machine requires four switching states, one per each x-y component, to fully cancel the average voltage production in x_1-y_1 and x_2-y_2 planes.

ii) Definition of switching states that will be used in each sector.

In order to create symmetrical VVs that sweep the whole α-β plane, the selection of the switching states can be done on the basis of the 18 sectors that are formed by the octadecagons O_1 to O_{10}. Taking as a criterion for the vector selection the maximization of the α-β voltage production and the minimization of x_1-y_1 and x_2-y_2 voltages, two

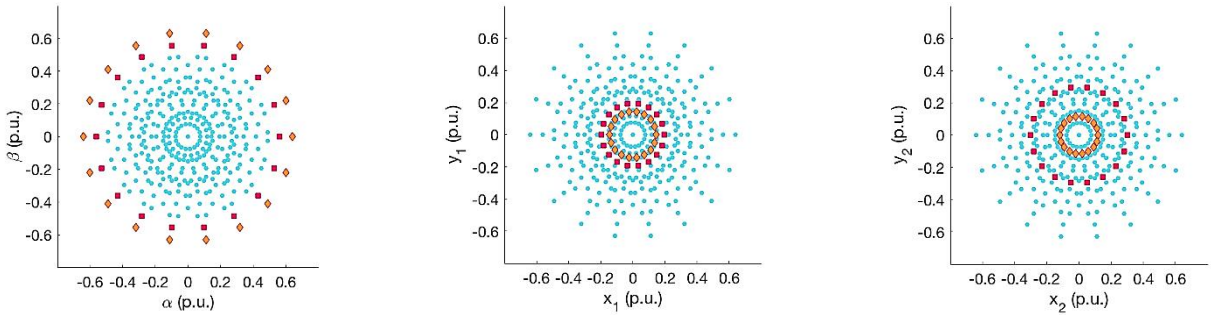

Fig. 2. Voltage vectors selected for the formation of virtual vectors and their projections in α-β, x_1-y_1 and x_2-y_2 subspaces.

consecutive pairs from O_1 and O_2 are selected (Fig. 3, left plots). For the sake of example, in sector 1 the first VV is formed from voltage vectors $v_1 = V_{450}$ of O_1 (cyan trace), $v_2 = V_{451}$ of O_2 (yellow trace), $v_3 = V_{449}$ of O_1 (orange trace) and $v_4 = V_{482}$ of O_2 (green trace). It can be noted that, apart from having a favourable individual value of $R_{\alpha\beta}$ (see Table I), the four selected vectors have a good spatial disposition because they are mostly aligned in the α-β plane (see Fig. 3a, left plot) and have opposite directions in the x_1-y_1 (Fig. 3b, left plot) and x_2-y_2 (Fig. 3c, left plot) planes.

iii) Calculation of the time of application of each switching state.

Once the four vectors per sector have been identified, it is time to determine the times of applications of these vectors so as to zero the x-y voltage production. If t_j is time of application of voltage vector j (with $j \in [1,2,3,4]$) and v_j^k is the k component ($k\epsilon[x_1, y_1, x_2, y_2]$) of voltage vector j, the condition of zero average voltage production in the x_1-y_1 and x_2-y_2 planes can be mathematically expressed as:

$$\begin{bmatrix} v_1^{x_1} & v_2^{x_1} & v_3^{x_1} & v_4^{x_1} \\ v_1^{y_1} & v_2^{y_1} & v_3^{y_1} & v_4^{y_1} \\ v_1^{x_2} & v_2^{x_2} & v_3^{x_2} & v_4^{x_2} \\ v_1^{y_2} & v_2^{y_2} & v_3^{y_2} & v_4^{y_2} \end{bmatrix} \cdot \begin{bmatrix} t_1 \\ t_2 \\ t_3 \\ t_4 \end{bmatrix} = \begin{bmatrix} 0 \\ 0 \\ 0 \\ 0 \end{bmatrix} \quad (4)$$

Since the determinant of (4) is zero, the system of equations is undetermined. This means that to nullify the x_1-y_1 and x_2-y_2 components it is sufficient to set a certain proportion of the times:

$$\begin{bmatrix} v_1^{x_1} & v_2^{x_1} & v_3^{x_1} \\ v_1^{y_1} & v_2^{y_1} & v_3^{y_1} \\ v_1^{x_2} & v_2^{x_2} & v_3^{x_2} \end{bmatrix} \cdot \begin{bmatrix} t_1/t_4 \\ t_2/t_4 \\ t_3/t_4 \end{bmatrix} = \begin{bmatrix} -v_4^{x_1} \\ -v_4^{y_1} \\ -v_4^{x_2} \end{bmatrix} \quad (5)$$

However, since these times have to be applied within a sampling period, the following restriction also has to be satisfied:

$$t_1 + t_2 + t_3 + t_4 = \mathrm{T_s} \quad (6)$$

where T_s is the sampling time. Equations (5)-(6) form a determined system and it is now possible to calculate the times of application t_j. For sector 1, the solution of (5)-(6) provides $t_1 = t_3 = 0.3082 \cdot T_s$ and $t_2 = t_4 = 0.1916 \cdot T_s$. The left plot in Fig. 3a shows that VV_1 yields a high modulus of the α-β voltage (specifically 93.9% of the magnitude of large vectors in O_1), whereas the vector sum of v_1, v_2, v_3 and v_4 provides zero average voltage in both x_1-y_1 and x_2-y_2 planes (left plots in Fig. 3b and 3c).

The $2^9 = 512$ switching states are located in 18 different sectors where voltage vectors are rotated but equally distributed (see Fig. 2). Hence the switching states are different in each sector (e.g. in sector II $v_1 = 449$, $v_2 = 482, v_3 = 481$ and $v_4 = 465$), but from symmetry considerations the times of application t_1, t_2, t_3 and t_4 remain the same (i.e. $t_1 = t_3 = 0.3082 \cdot T_s$ and $t_2 = t_4 = 0.1916 \cdot T_s$). Following this procedure, it is possible to obtain 18 VVs formed by four switching states (one per sector) according to:

$$VV_s(v_1, v_2, v_3, v_4) = v_1 \cdot t_1 + v_2 \cdot t_2 + v_3 \cdot t_3 + v_4 \cdot t_4 \quad (7)$$

With the aforementioned selection procedure and using (5)-(7), it is possible to create the 18 VVs, which are symmetrically located in the α-β plane and provide high α-β voltage production and zero x-y voltage (see Fig. 4, left plots).

C. *Virtual voltage vectors using two switching states (2-VV)*

Even though the 4-VVs that have been obtained in section II.B exactly cancel the x_1-y_1 and x_2-y_2 components, the use of four switching states increases the effective switching frequency of the VSC. It is then prudent to examine if a suboptimal solution based on less switching states might be good enough in practice. This section explores the possibility to create VVs with only two switching states. It is firstly noted that the voltage vectors in octadecagons O_1 and O_2 are aligned in pairs in the α-β plane (Fig. 2, left plot). For the sake of example, in sector 1 the voltage vectors $v_1 = V_{450}$ of O_1 and $v_2 = V_{451}$ of O_2 are aligned in the α-β plane and

TABLE I

MODULUS OF VOLTAGE VECTORS IN EACH SUBSPACE OF VSD, α-β RATIO AND PERCENTAGE OF α-β CONTRIBUTION CONSIDERING THE MAXIMUM α-β RATIO AS 100%. ALL VALUES GIVEN FOR EACH OCTADECAGON.

Values	O_1	O_2	O_3	O_4	O_5	O_6	O_7	O_8	O_9	O_{10}
$\lvert v_{\alpha\beta}\rvert \cdot 10^2$	64	56	42	34	30	22	20	15	12	8
$\lvert v_{x_1y_1}\rvert \cdot 10^2$	15	20	8	42	56	22	30	12	64	34
$\lvert v_{x_2y_2}\rvert \cdot 10^2$	12	30	34	8	20	22	56	64	15	42
$R_{\alpha\beta}$	3.3	1.5	1.2	0.8	0.5	0.7	0.3	0.23	0.18	0.15
%	**100**	**46**	**36**	**24**	**15**	**21**	**9**	**7**	**5**	**4**

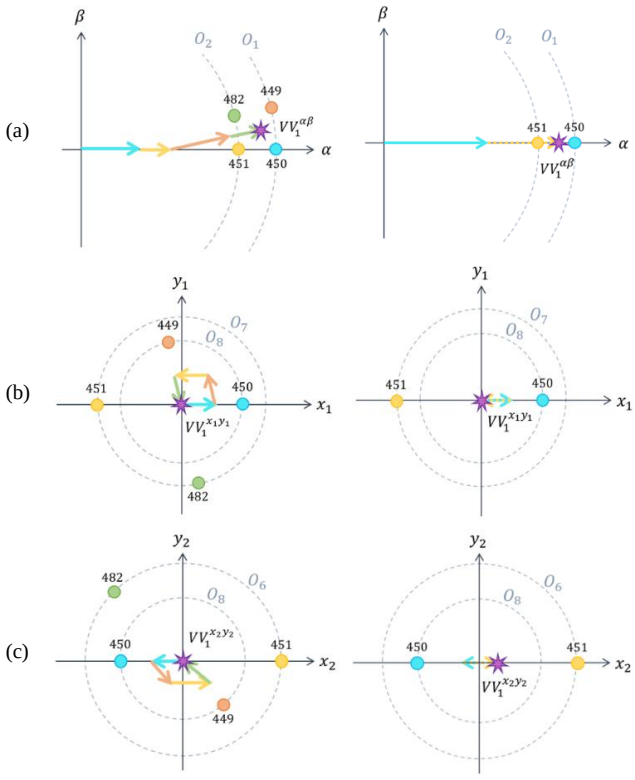

Fig. 3. Construction of VV_1 using 4-VV (left plots) and 2-VV (right plots) shown in a) α-β subspace, c) x_1-y_1 subspace and c) x_2-y_2 subspace.

might be combined to generate a VV with high α-β magnitude (Fig. 3a, right plot). Fortunately, the selected voltage vectors $v_1 = V_{450}$ and $v_2 = V_{451}$ happen to be in opposite directions in both x_1-y_1 and x_2-y_2 planes. It is thus confirmed that v_1 and v_2 have ideal disposition for the purpose of VVs, i.e. they maximize α-β components while minimizing the x-y contribution.

In spite of the good disposition of vectors v_1 and v_2 it is not possible to achieve a null average voltage in both subspaces. It is then necessary to select one out of three possible criteria: *i)* cancelling the secondary components in the x_1-y_1 plane, *ii)* cancelling the secondary components in the x_2-y_2 plane or *iii)* minimizing the secondary components in both the x_1-y_1 and x_2-y_2 planes. Since the plane x_1-y_1 contains lower-order harmonics, the first criterion is the chosen one in this work to calculate the times of applications of voltage vectors v_1 and v_2. Imposing the x_1-y_1 voltage cancellation and the restriction of the sampling time the system of equations is:

$$\begin{aligned} v_1^{x_1} \cdot t_1 + v_2^{x_1} \cdot t_2 &= 0 \\ v_1^{y_1} \cdot t_1 + v_2^{y_1} \cdot t_2 &= 0 \\ t_1 + t_2 &= T_s \end{aligned} \tag{8}$$

As in section II.B, the first two equations are linearly dependent and consequently (8) provides an undetermined solution. For sector 1, the times of application of voltage vectors $v_1 = V_{450}$ of O_1 and $v_2 = V_{451}$ of O_2 are $t_1 = 0.574 \cdot T_s$ and $t_2 = 0.426 \cdot T_s$. Once the application times have been obtained, it is now possible to generate the virtual vector as:

$$VV_1(v_1, v_2) = v_1 \cdot t_1 + v_2 \cdot t_2 \tag{9}$$

The alignment of voltage vectors v_1 and v_2 results in a high magnitude of VV_1 in the α-β plane (specifically 94.9% of the magnitude of large vectors in O_1), as it is shown in Fig. 3a, right plot. Since the times of application have been set according to (8) the average voltage in the x_1-y_1 plane is exactly zero, whereas in this case the average voltage in the x_2-y_2 plane is non-zero, but low (specifically 9.3% of the magnitude of large vectors in O_1). Right plots in Fig. 3b and 3c show the performance of 2-VVs in the secondary planes, where the full cancellation is not fully achieved. By extending the procedure to all sectors, it is possible to create 18 vectors formed by just two switching states (2-VVs) that are symmetrically located (see Fig. 4, right plots).

As a summary, the created 2-VVs have a slightly higher magnitude than 4-VV in the α-β, the same voltage production in the x_1-y_1 (i.e. zero), and non-zero but low x_2-y_2 voltage production. Since the voltage harmonics mapped in the x_2-y_2 plane have higher order, the parasitic currents will be limited to some extent due to the inductive nature of the machine. On the other hand, the 2-VVs are simpler to implement and will provide lower switching frequency, as it will be experimentally shown in section V.

Proposed virtual vectors (either 4-VV or 2-VV) can be used both in MPC and DTC control strategies. A brief description of the control methods that will be later on used in the experiments is included next.

III. MODEL PREDICTIVE CONTROL

Model predictive control is recently a popular strategy for the current regulation of multiphase drives. Besides having a simple structure and fast dynamic response, new constraints can be easily added due to the intrinsic flexibility of the control structure. Within the so-called predictive control family, the finite-control set version (simply termed MPC for simplicity in what follows) has been widely studied in field of multiphase drives, [31], [32], [34]. It is also adopted in this work to prove the goodness of the VVs proposed in the previous section. MPC algorithm takes advantage of the limited number of switching states of the converter to estimate the future states and select the most suitable control output [35].

The MPC scheme is shown in Fig. 5. The predictive model (a discrete version of the machine model [36]) takes the measured currents and mechanical speed as inputs and generates a prediction of the VSD currents in the next sampling period for each voltage input. While in standard MPC the voltage inputs are the switching states of the converter, in the current VV-based version of MPC the voltage inputs are the averaged values of the VVs (either 4-VV or 2-VV). Predicted currents are compared to reference currents coming from the outer speed loop and flux settings.

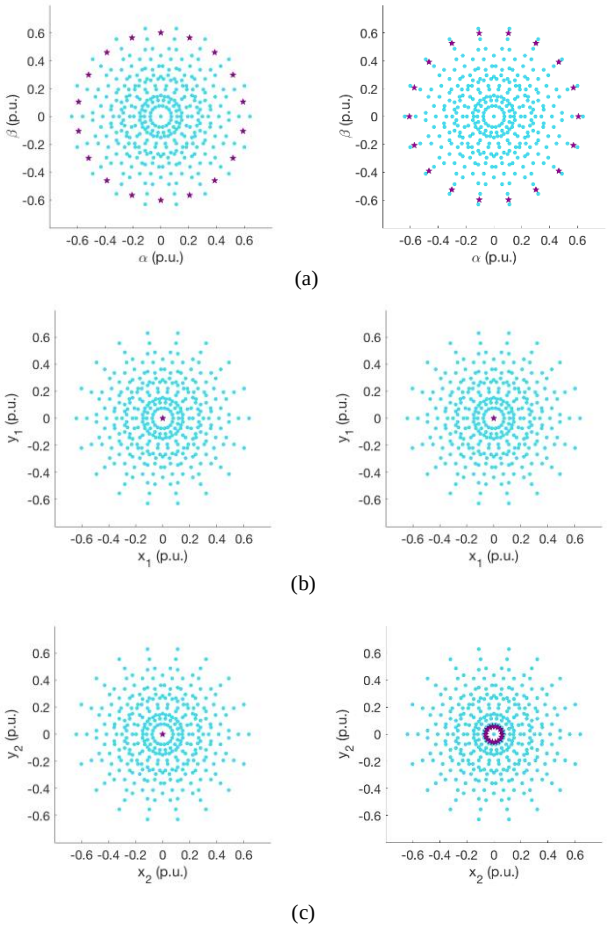

Fig. 4. Mapping of virtual vectors in different subspaces considering 4-VV (left plots) and 2-VV (right plots). From top to bottom: a) Virtual vectors in α-β subspace, b) virtual vectors in x_1-y_1 subspace and c) virtual vectors in x_2-y_2 subspace.

The performance is evaluated with a predefined cost function:

$$\begin{aligned} J_k &= e_{\alpha\beta} + K_{x_1y_1} \cdot e_{x_1y_1} + K_{x_2y_2} \cdot e_{x_2y_2} \\ e_{\alpha\beta} &= (i_\alpha^* - \hat{\imath}_\alpha)^2 + \left(i_\beta^* - \hat{\imath}_\beta\right)^2 \\ e_{x_1y_1} &= \left(i_{x_1}^* - \hat{\imath}_{x_1}\right)^2 + \left(i_{y_1}^* - \hat{\imath}_{y_1}\right)^2 \\ e_{x_2y_2} &= \left(i_{x_2}^* - \hat{\imath}_{x_2}\right)^2 + \left(i_{y_2}^* - \hat{\imath}_{y_2}\right)^2 \end{aligned} \quad (10)$$

where k is one of the 19 possible switching states (18 active vectors from octadecagon O_1 plus the zero vector) in standard MPC or one of the 19 VVs (18 active VVs plus the zero vector) in the VV-based version of MPC. $K_{x_jy_j}$ coefficients are the weighting factors for the regulation of the secondary plane components. They are experimentally tuned by trial and error procedure using the criterion to keep x_1-y_1 and x_2-y_2 currents around zero with low current ripple and, at the same time, avoid any significant disturbance in the α-β plane that could affect the flux/torque production [32].

IV. DIRECT TORQUE CONTROL

Direct torque control strategy is also a widely used control strategy to regulate the speed of electric machines. This strategy also lacks a modulation stage and it is remarkable for its simplicity and robustness. The torque and the flux are the control variables, which are controlled independently with fast dynamics.

To implement DTC, the first step is to estimate the torque and flux of the machine. This is accomplished here using the measured phase currents and mechanical speed (see Fig. 6). As in MPC, the estimation is done with a discrete time model of the machine [36]. The only difference is that while in the DTC it is simply necessary to estimate the α-β rotor flux, MPC also requires the estimation of the α-β rotor currents. Next, after comparing the estimated control variables with their references, two hysteresis controllers are used, one with five levels for the torque regulation and another one with two levels for the flux control. The bandwidths of the controllers are defined taking into account the magnitudes of the variables to be controlled. This, together with the identification of the sector where flux is located, will determine the optimal selection of the switching states of the converter.

It must be noted that, as mentioned previously, in order to achieve a correct regulation of the secondary currents, the virtual voltage vectors will be used. These are selected in the look-up table once the control action is decided.

V. RESULTS

A. Test bench

The test bench shown in Fig. 7 has been used to make a series of experimental tests. It consists of a nine-phase induction machine which has been rewound to obtain an asymmetrical nine-phase winding. This machine is driven by two custom-made converters (based on Infineon FS50R12KE3 IGBT modules) connected to a dc source (PAS2500 linear amplifier) provided by Spitzenberger & Spies. On the other hand, the nine-phase induction machine is mechanically coupled to a dc machine by the Magtrol TM 210 torque meter. To operate as a generator, the dc machine is connected to a passive load. To the contrary, if the desirable operating mode is as a motor, the dc machine is supplied by the Sorensen SGI600/25 power supply system. Finally, the proposed control method is programmed using a dSPACE platform, which also carries out the measurements of the control variables. The phase currents are measured by converters' internal LEM sensors and acquired by a ADC board, while the speed and position are provided by an incremental encoder board which captures signals and is mounted on the shaft of the nine-phase machine. The motor parameters are shown in Table II.

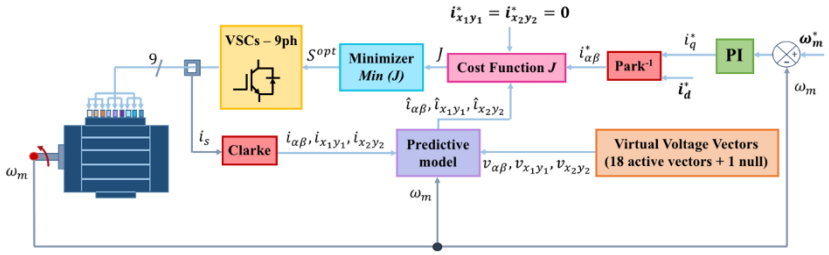

Fig. 5. FCS-MPC scheme with VVs for an asymmetrical nine-phase induction machine.

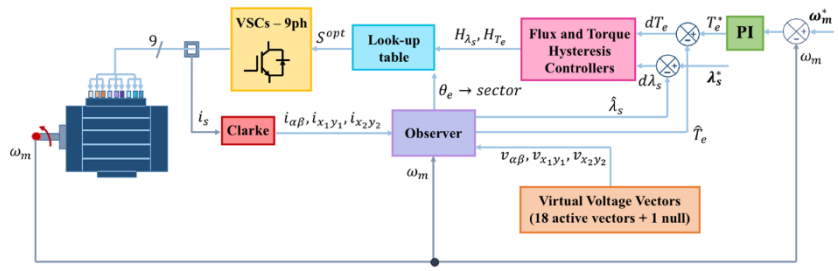

Fig. 6. DTC scheme with VVs for an asymmetrical nine-phase induction machine.

B. *Experimental results*

This section includes steady state (tests 1-2) and dynamic (tests 3-4) experimental results obtained with the MPC and DTC. Test 1 verifies the steady state performance of standard MPC, 2-VV MPC and 4-VV MPC (Fig. 8). In this test the machine rotates at 1000 rpm with a load torque of -2.4 Nm (see Fig 8h), a dc-link voltage of 500 V and a d-current reference of 1.9 A. It can be observed that all three approaches satisfactorily regulate the motor speed (Fig. 8a) with minimum differences in the d-q current tracking (Fig. 8b and 8c). The appearance of x_1-y_1 and x_2-y_2 currents is very similar with the use of VVs (Fig. 8d and 8e), and the differences are not remarkable. Two reasons explain this fact:

- The stator leakage inductance is relatively high. While in [28] the ratio $100 \cdot L_{ls}/L_m = 0.36\%$, in this experimental rig it is approximately ten times higher ($100 \cdot L_{ls}/L_m = 4.6\%$). The higher value of the stator leakage inductance limits to some extent the magnitude of x-y currents when x-y voltages are non-zero.
- The MPC strategy indirectly regulates the x-y currents by means of the cost function. If the weighting factors of the cost function in (10) are set to high values (they have been set to $K_{xy1} = K_{xy2} = 1$ in standard MPC and 2-VV MPC), then the predictive algorithm will also account for the x_1-y_1 and x_2-y_2 currents and consequently reduce the amount of secondary currents. Only in the case of 4-VV MPC the weighting factors have been selected with a zero value (since all 4-VVs provide the zero voltages in the *x-y* planes).

The phase currents are finally depicted in Fig. 8f, showing a limited improvement of 2-VV and 4-VV over standard MPC. For the sake of quantification, the THD of MPC, 2-VV MPC and 4-VV MPC is 42.29%, 32.83%, and 31.22%, respectively. The main conclusion of test 1 is that VV-based methods have a limited capability to improve the current quality in this specific experimental setting. Considering that the switching frequency using VVs is higher (3800 Hz for 2-VV MPC, 4767 Hz for 4-VV MPC and 3070 Hz for MPC), it follows that the use of 2-VV and 4-VV does not outperform standard MPC when the stator leakage inductance is relatively high.

Test 2 examines the steady state performance of standard DTC, 2-VV DTC and 4-VV DTC (Fig. 9). Table III shows the gains of the regulators in these three versions of DTC. In this test the machine rotates at 1000 rpm with a load torque of 4 Nm, a dc-link voltage of 300 V and a stator flux reference equal to 0.988 Wb (rated flux). It can be observed that the three methods can satisfactorily regulate the motor speed (Fig. 9a) with similar flux and torque tracking capability (Fig. 9b and 9c). In the same way, the α-β currents also remain similar in the three methods under comparison (Fig. 9f) because there are no significant differences in the current control of the α-β plane. Nevertheless, the DTC strategy completely disregards the x-y planes and this leaves the x_1-y_1 and x_2-y_2 currents uncontrolled. This is noticeable

TABLE II
PARAMETERS USED FOR THE ASYMMETRICAL NINE-PHASE INDUCTION MACHINE

Parameters	Values	Units
Stator resistances, $R_{s\alpha\beta}$, $R_{sx_1y_1}$ and $R_{sx_2y_2}$	5.3	Ω
Rotor resistance, R_r	2.0	Ω
Stator leakage inductances, $L_{ls\alpha\beta}$, $L_{lsx_1y_1}$ and $L_{lsx_2y_2}$	24.0	mH
Rotor leakage inductance, L_{lr}	11.0	mH
Mutual inductance, L_m	520.0	mH
Number of pole pairs, p	1	–
Number of neutral points, n	3	–
Rated current, I_n	2.5	A
Stator rated flux, λ_s^*	0.988	Wb
Rated torque, T_n	7	N·m
Sampling frequency, f_m	10	kHz

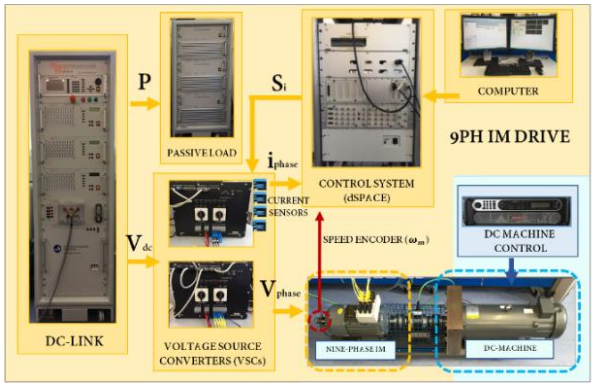

Fig. 7. Test bench.

TABLE III
GAINS OF THE REGULATORS (PI AND HYSTERESIS BANDS) FOR MPC AND DTC

MPC and DTC controllers			
PI_ω		HB	
K_p	3	H_{Te_1}	0.1
		H_{Te_2}	0.2
K_i	30	$H_{\lambda s}$	0.01

in the left plot of Figs. 8d and 8e, where high current ripples exist, even though the impedance in the x-y planes is relatively high. To the contrary, the use of 2-VV and 4-VV highly restricts the ripple magnitude of x_1-y_1 and x_2-y_2 currents (Fig. 9d and 9e, middle and right plots) because the VVs indirectly regulate the x-y currents in an open-loop mode by having a zero x-y voltage production. The lack of x-y control in standard DTC and the high x-y current ripple lead to poor phase current waveforms (Fig. 9g, left plots) that will generate additional copper losses and consequently lower efficiency. It is found however that the use of 2-VV and 4-VV DTC significantly improves the waveforms of phase currents (Fig. 9g, middle and right plots).

Aiming to further quantify the improvement in the phase current quality, the rms value, THD and spectrum of the phase currents shown in Fig. 9g are calculated next. While the THD in DTC is 98.4%, this value is reduced to 30.96%

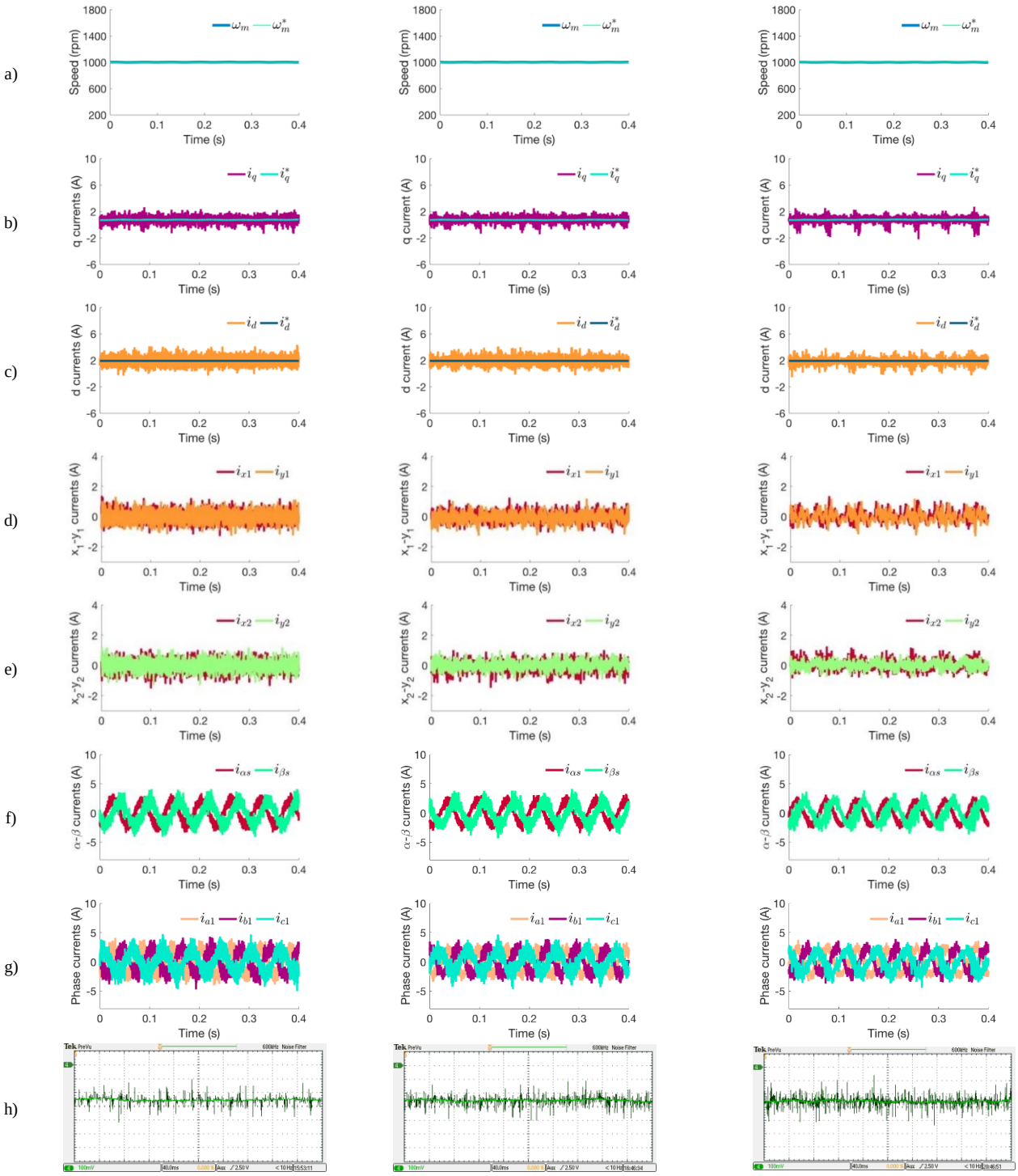

Fig. 8. Steady state test for the standard FCS-MPC (left plots), FCS-MPC with 2-VV (middle plots) and FCS-MPC with 4-VV (right plots). From top to bottom: a) motor speed, b) d-currents, c) q-currents, d) x_1-y_1 currents, e) x_2-y_2 currents, f) α-β currents, g) $a_1 b_1 c_1$ phase currents and h) measured torque.

and 30.82% in 2-VV and 4-VV DTC, respectively. In the spectrum shown in the left plot of Fig. 10 it can be observed that DTC has a high amount of the 5^{th} and 7^{th} harmonics, this being precisely those harmonics mapped in the x-y planes (5^{th} is mapped in x_1-y_1 whereas 7^{th} is mapped into x_2-y_2). It is thus confirmed that the highly distorted phase current waveform of Fig. 9g is caused by the current harmonics mapped in the x-y planes. The current harmonics are however well limited with the use of VVs, as it is shown in the middle and right plots of Fig. 10 (the 5^{th} is reduced by 71.36% and 51.64% and the 7^{th} is reduced by 83.39% and 82.23% with 2-VV and 4-VV DTC, respectively).

Finally, the rms value of the phase current is 1.85 A, 1.56 A and 1.58 A for standard DTC, 2-VV and 4-VV DTC,

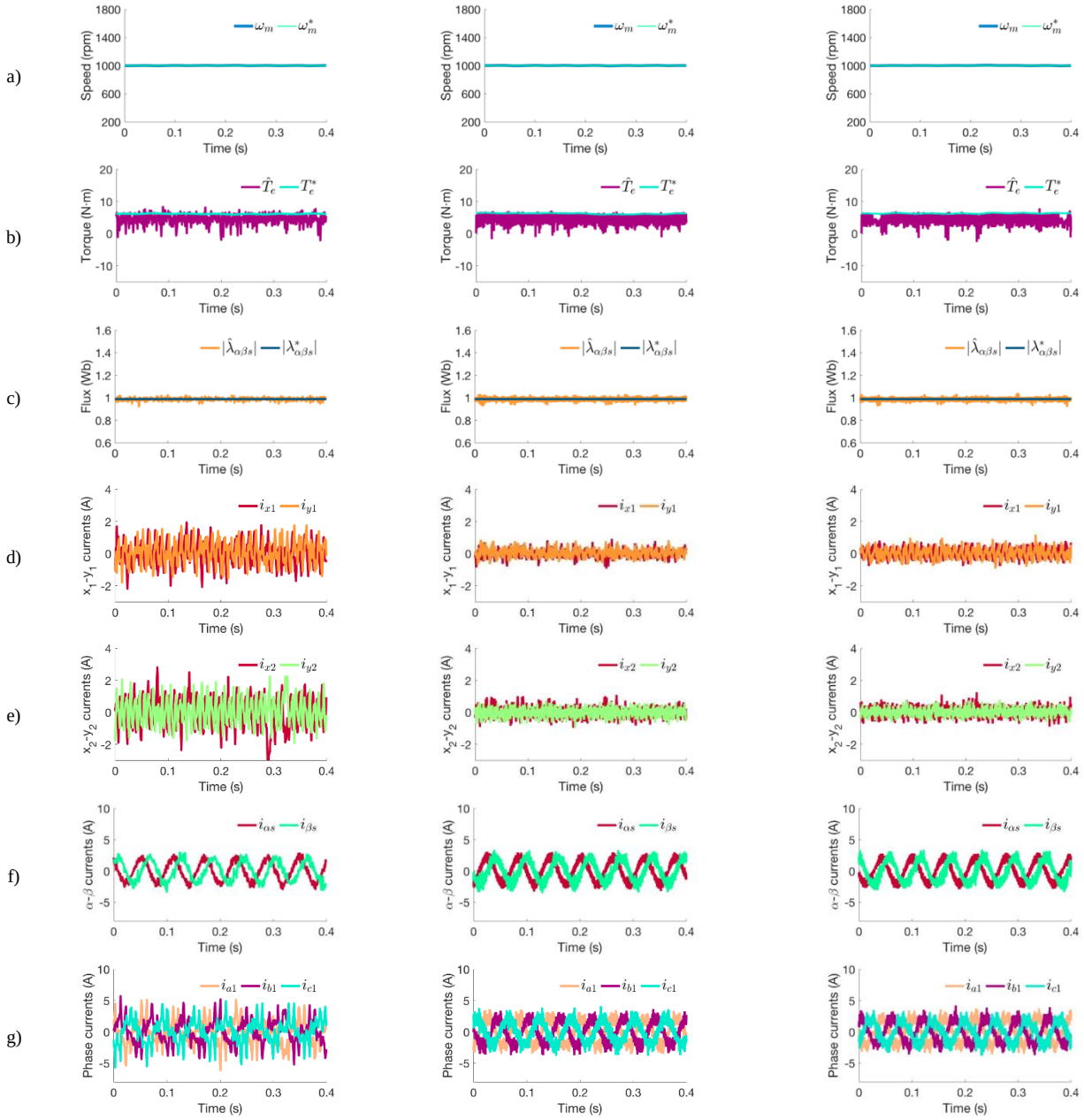

Fig. 9. Steady state test for the standard DTC (left plots), DTC with 2-VV (middle plots) and DTC with 4-VV (right plots). From top to bottom: a) motor speed, b) electromagnetic torque, c) modulus of the α-β stator flux, d) x_1-y_1 currents, e) x_2-y_2 currents, f) α-β currents and g) $a_1b_1c_1$ phase currents.

leading to a reduction of the stator copper losses by 28.9% and 27.5% when using 2-VV and 4-VV, compared to standard DTC. The current quality improvement comes at the price of increasing the switching frequency in 2-VV DTC (3712 Hz) and 4-VV DTC (4559 Hz).

Some conclusions can be extracted from tests 1 and 2:

- The use of VVs together with MPC is only worthy if the impedance of the x-y planes is low enough to generate a significant amount of x-y currents. Otherwise, it is simpler and beneficial to use standard MPC.
- Unlike MPC, standard DTC does not present favorable operating conditions due to its inability to regulate the x_1-y_1 and x_2-y_2 currents. In spite of the relatively high x-y impedance, the highly distorted phase currents lead to unacceptable values of the current THD and lower overall efficiency.
- The use of VVs together with DTC allows preserving the satisfactory flux and torque control while keeping x-y currents low. The current THD and stator copper losses can be reduced by around 70% and 30%, respectively.
- The use of 4-VV and 2-VV bring similar performance in practice in spite of the non-zero voltage production in the x_2-y_2 plane of the latter. Since 2-VV is simpler to implement in practice and provides lower switching frequency, it is a preferred solution compared to the use of 4-VV.

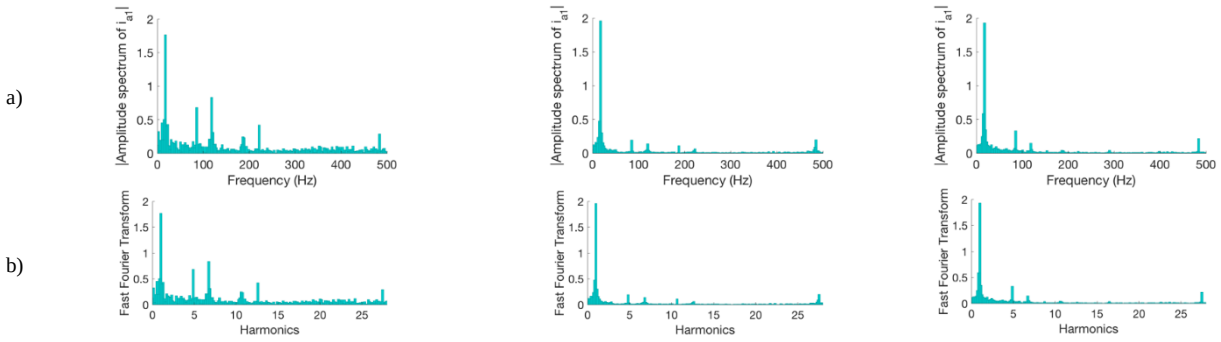

Fig. 10. Analysis of the current quality in steady state for the standard DTC (left plots), DTC with 2-VV (middle plots) and DTC with 4-VV (right plots). From top to bottom: a) frequency spectrum of the a_1 phase current and b) harmonics of the a_1 phase current.

- It is advisable to use 2-VV together with DTC in all cases whereas it is interesting to use 2-VV together with MPC only when the impedance of the x-y plane is low enough to distort the current significantly [32].

Since the steady-state performance has been analyzed in tests 1 and 2, the dynamic performance of 2-VV and 4-VV using MPC and DTC is evaluated next.

Tests 3 and 4 use a speed ramp as the reference and include 2VV-based MPC and DTC, respectively (see Figs. 11 and 12). In test 3 the dc-link voltage and d-current reference are set to 500 V and 1.9 A, respectively. The speed reference is ramped from 500 rpm to 1500 rpm in generating mode with a load torque of -5 Nm. Fig. 11g shows the evolution of the measured torque in test 3, where the machine is operating in generating mode. The speed regulation during the transient is satisfactory (Fig. 11a), the d-current is properly tracked and unaffected by the dynamic condition (Fig. 11b) and the q-current is correctly tracked during the acceleration and deceleration transients (Fig. 11c). The x_1-y_1 and x_2-y_2 currents are kept low and with constant ripple regardless of the variable torque and flux conditions (Figs. 11d and 11e). The α-β currents depicted in Fig. 11f have the expected standard waveform with increasing frequency as the motor accelerates. Summarizing, test 3 results confirm the ability of 2-VV MPC to handle dynamic conditions and retain good and decoupled x-y current control.

In test 4 (see Fig. 12) the dc-link voltage is set to 300 V and the stator flux is equal to its rated value of 0.988 Wb. Here there is a reference speed change from 500 rpm to 1250 rpm in generating mode with a load torque of -4 Nm. The speed and torque (Figs. 12a and 12b) track their respective references properly and the flux is well regulated to its rated value (Fig. 12c). Referring to the x_1-y_1 and x_2-y_2 currents (Fig. 12d and 12e), whose magnitudes are also not affected by the speed increase. As for the α-β currents (Fig. 12f), the acceleration of the machine is reflected in their frequencies.

The main conclusion after the dynamic test for MPC (test 3) and DTC (test 4) is that the control methods based on 2-VV retain a satisfactory performance during transients with decoupled x_1-y_1 and x_2-y_2 currents. The use of 2-VV MPC and DTC ensures good dynamics with simpler implementation and lower switching frequency.

VI. CONCLUSIONS

Control strategies without a modulation stage (e.g. MPC and DTC) cannot ensure zero voltage production in the secondary planes (x_1-y_1 and x_2-y_2 subspaces). If the leakage inductance in those planes is high enough, the application of a finite-control set MPC is a feasible option since the x_1-y_1 and x_2-y_2 can be reasonably limited. The MPC indirectly regulates the secondary planes by including x_1-y_1 and x_2-y_2 terms in the cost function that allow an acceptable performance. However, the DTC strategy does not take into account the x_1-y_1 and x_2-y_2 subspaces, and this results in an unacceptable phase current ripple that leads to poor efficiency and high THD.

In order to overcome the limitations of DTC (in all cases) and MPC (when the leakage inductance is low), virtual vectors (VVs) are used to regulate in an open-loop mode the x_1-y_1 and x_2-y_2 voltages and this keeps the x_1-y_1 and x_2-y_2 current ripple at low values. Nullifying both x_1-y_1 and x_2-y_2 voltages requires the use of four switching states during the sampling period, but it is possible to cancel the x_1-y_1 voltage and keep the x_2-y_2 voltage at very low values just by applying two switching states. The 2-VV strategy provides a similar performance as 4-VV, but with simpler implementation and lower switching frequency.

Compared to standard DTC, the proposed 2-VV DTC reduces the 5^{th} current harmonics by 71.36% and the 7^{th} current harmonic by 83.39%, which in turn makes the current THD 70% lower and the stator copper losses 30% lower. At the same time the good dynamic performance is preserved with good decoupling and low ripple of the the x_1-y_1 and x_2-y_2 currents.

The theoretical contributions of this work confirm that it is possible to create optimal (4-VV) and suboptimal (2-VV) virtual vectors that can be applied either with MPC or DTC strategies, and the experimental validation highlights the improvements in terms of power quality and efficiency that can be obtained in DTC. The concept is also applicable to MPC, but its practical benefits are limited to nine-phase machines with low impedance in the secondary planes.

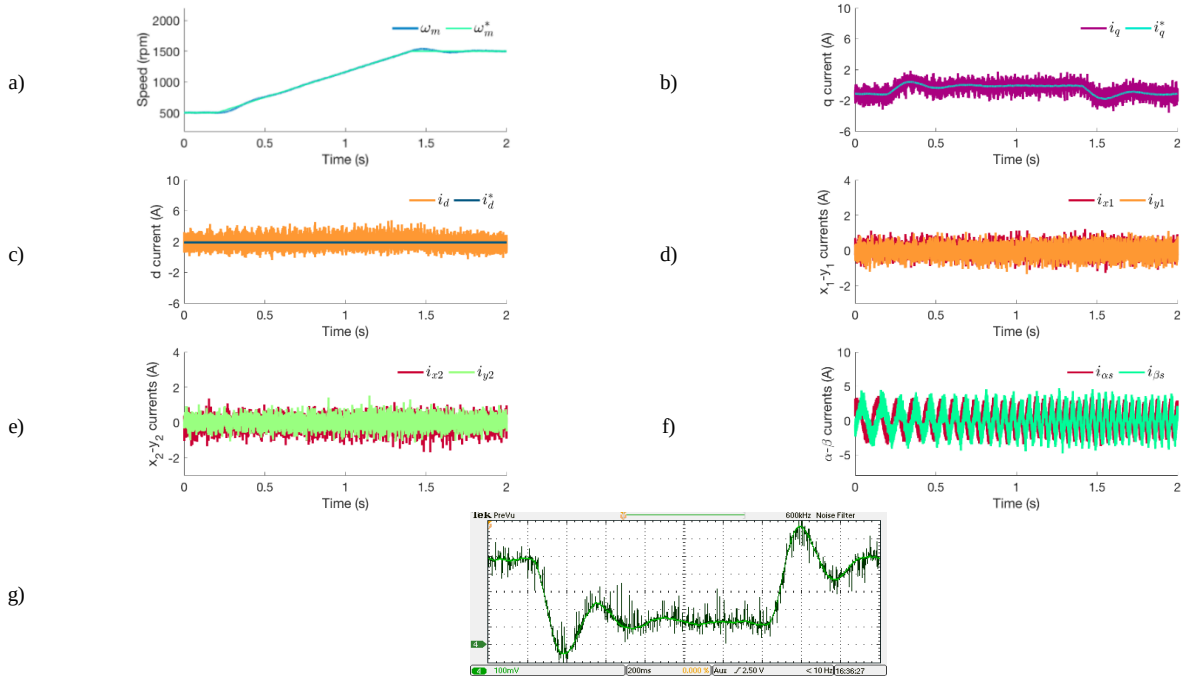

Fig. 11. Dynamic test with a ramped speed reference for the FCS-MPC with 2-VV. From top to bottom and from left to right: a) Motor speed, b) d-currents, c) q-currents, d) x_1-y_1 currents, e) x_2-y_2 currents, f) α-β currents and g) measured torque.

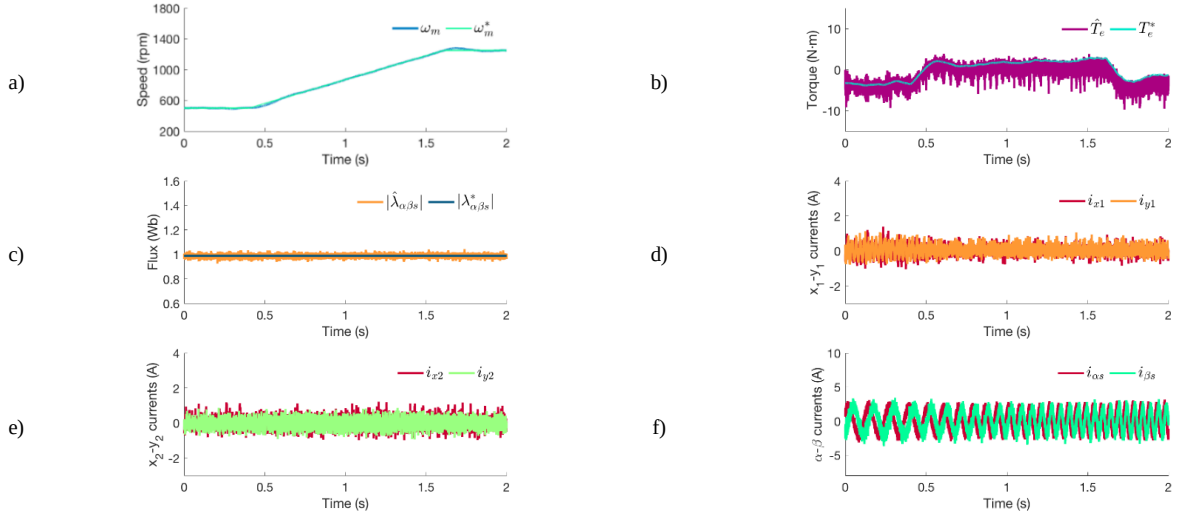

Fig. 12. Dynamic test with a speed ramp reference for the DTC with 2-VV. From top to bottom and from left to right: a) motor speed, b) electromagnetic torque, c) modulus of the α-β stator flux, d) x_1-y_1 currents, e) x_2-y_2 currents and f) α-β currents.

REFERENCES

[1] F. Barrero and M.J. Duran, "Recent advances in the design modeling, and control of multiphase machines – Part I", *IEEE Transactions on Industrial Electronics*, vol. 63, no. 1, pp. 449-458, 2016.

[2] M.J. Duran and F. Barrero, "Recent Advances in the design modelling, and control of multiphase machines – Part II", *IEEE Transactions on Industrial Electronics*, vol. 63, no. 1, pp. 459-468, 2016.

[3] E. Levi, "Advances in converter control and innovative exploitation of additional degrees of freedom for multiphase machines", *IEEE Transactions on Industrial Electronics*, vol. 63, no. 1, pp. 433-448, 2016.

[4] M. Benatmane and T. McCoy, "Development of a 19 MW PWM converter for U.S. Navy surface ships", *International Conference on Electric Ship (ELECSHIP)*, Istanbul, Turkey, pp. 109-113, 1998.

[5] T. McCoy and M. Benatmane, "The all-electric warship: An overview of the U.S. Navy's integrated power system development programme", *International Conference on Electric Ship (ELECSHIP)*, Istanbul, Turkey, pp. 1-4, 1998.

[6] C.L. Ferreira and R.W.G. Bucknall, "Modelling and real-time simulation of an advanced marine full-electrical propulsion system" *Second International Conference on Power Electronics, Machines and Drives*, Edinburgh, U.K., no. 498, 2004.

[7] C. Hodge, S. Williamson and A.C. Smith, "Direct drive marine propulsion motors", *Proceedings International Conference on Electrical Machines*, Bruges, Belgium, no. 807, 2002.

[8] S. Lu and K. Corzine, "Multilevel multi-phase propulsion drives", *IEEE Electric Ship Technologies Symposium*, Philadelphia, PA, pp. 363-370, 2005.

[9] M.G. Simoes and P. Vieira, "A high-torque low-speed multiphase brushless machine – A perspective application for electric vehicles" *IEEE Transactions on Industrial Electronics*, vol. 49, no. 5, pp. 1154-1164, 2002.

[10] S.D. Sudhoff, J.T. Alt, N.J. Hegner and H.N.Jr. Robey, "Control of a 15-phase induction motor drive system", *Proceedings Naval Symposium Electric Machines*, Newport, RI, pp. 69-75, 1997.

[11] S. Smith, "Developments in power electronics, machines and drives", *IEEE Power Engineering Journal*, vol. 16, no. 1, pp. 13-17, 2002.

[12] F. Terrien, S. Siala and P. Noy, "Multiphase induction motor sensorless control for electric ship propulsion", *Second International Conference on Power Electronics, Machines and Drives*, Edinburgh, U.K. no. 498, 2004.

[13] E. Levi, "Advances in converter control and innovative exploitation of additional degrees of freedom for multiphase machines", *IEEE Transactions on Industrial Electronics*, vol. 63, no. 1, pp. 433-448, 2016.
[14] H.S. Che, E. Levi, M. Jones, M.J. Duran W.P. Hew and N.A. Rahim, "Operation of a six-phase induction machine using series-connected machine-side converters", *IEEE Transactions on Industrial Electronics*, vol. 61, no. 1, pp. 164-176, 2014.
[15] M.J. Duran, I. Gonzalez-Prieto, A. Gonzalez-Prieto and F. Barrero, "Multiphase energy conversion systems connected to microgrids with unequal power-sharing capability", *IEEE Transactions on Energy Conversion*, vol. 32, no. 4, pp. 1386-1395, 2017.
[16] I. Subotic, N. Bodo and E. Levi, "Single-phase on-board integrated battery chargers for EVs based on multiphase machines", *IEEE Transactions on Power Electronics*, vol. 31, no. 9, pp. 6511-6523, 2016.
[17] A. Tani, M. Mengoni, L. Zarri, G. Serra and D. Casadei, "Control of multiphase induction motors with an odd number of phases under open-circuit phase faults", *IEEE Transactions on Power Electronics*, vol. 27, no. 2, pp. 565-577, 2012.
[18] M.J. Duran, I. Gonzalez-Prieto, F. Barrero, E. Levi, L. Zarri and M. Mengoni, "A simple braking method for six-phase induction motor drives with unidirectional power flow in the base-speed region", *IEEE Transactions on Industrial Electronics*, vol. 64, no. 8, pp. 6032-6041, 2017.
[19] H.S. Che, E. Levi, M. Jones, W.P. Hew and N.A. Rahim, "Current control methods for an asymmetrical six-phase induction motor drive", *IEEE Transactions on Power Electronics*, vol. 29, no. 1, pp. 407-417, 2014.
[20] M.J. Duran, E. Levi and F. Barrero, *Multiphase Electric Drives: Introduction*, Wiley Encyclopedia of Electrical and Electronics Engineering, John Wiley and Sons, pp. 1–26, 2017.
[21] L. Zheng, J.E. Fletcher, B.W. Williams and X. He, "A novel direct torque control scheme for a sensorless five-phase induction motor drive", *IEEE Transactions on Industrial Electronics*, vol. 58, no. 2, pp. 503-513, 2011.
[22] M. Bermudez, I. Gonzalez-Prieto, F. Barrero, H. Guzman, M.J. Duran and X. Kestelyn, "Open-phase fault-tolerant direct torque control technique for five-phase induction motor drives*", IEEE Transactions on Industrial Electronics*, vol. 64, no. 2, pp. 902-911, 2017.
[23] L. Gao, J.E. Fletcher and L. Zheng, "Low-speed control improvements for a two-level five-phase inverter-fed induction machine using classic direct torque control", *IEEE Transactions on Industrial Electronics*, vol. 58, no. 7, pp. 2744-2754, 2011.
[24] R. Kianinezhad, B. Nahid, F. Betin and G.A. Capolino, "A novel direct torque control (DTC) method for dual three phase induction motors", *IEEE International Conference on Industrial Technology*, 2006.
[25] R. Kianinezhad, R. Alcharea, B. Nahid, F. Betin and G.A. Capolino, "A novel direct torque control (DTC) for six-phase induction motors witch common neutrals", *IEEE International Symposium on Power Electronics, Electrical Drives, Automation and Motion*, 2008.
[26] J.K. Pandit, M.V. Aware, R.V. Nemade and E. Levi, "Direct torque control scheme for a six-phase induction motor with reduced control ripple", *IEEE Transactions on Power Electronics*, vol. 32, no. 9, pp. 7118-7129, 2017.
[27] J.K. Pandit, M.V. Aware, R.V. Nemade and Y. Tatte, "Direct torque control of asymmetric six-phase induction motor with reduction in current harmonics", *IEEE International Conference on Power Electronics, Drives and Energy Systems*, 2016.
[28] P.G. Entrambasaguas, I. Gonzalez-Prieto, M.J. Duran, M. Bermudez and F. Barrero, "Direct torque control based on virtual voltage vectors for a six-phase induction machine", *Revista Iberoamericana de Automatica e Informatica Industrial*, vol. 15, no. 3, pp. 277-285, 2018.
[29] Y. Ren and Z.Q. Zhu, "Enhancement of steady-state performance in direct-torque-controlled dual three-phase permanent-magnet synchronous machine drives with modified switching table" *IEEE Transactions on Industrial Electronics*, vol. 62, no. 6, pp. 3338-3350, 2015.
[30] Y. Ren and Z.Q. Zhu, "Reduction of both harmonic current and torque ripple for dual three-phase permanent-magnet synchronous machine using modified switching-table-based direct torque control", *IEEE Transactions on Industrial Electronics*, vol. 62, no. 11, pp. 6671-6683, 2015.
[31] C. Xue, W. Song and X. Feng, "Finite control-set model predictive current control of five-phase permanent-magnet synchronous machine based on virtual voltage vectors", *IET Electric Power Applications*, vol. 11, no. 5, pp. 836-846, 2017.
[32] I. Gonzalez-Prieto, M.J. Duran, J.J. Aciego, C. Martin and F. Barrero, "Model predictive control of six-phase induction motor drive using virtual voltage vectors", *IEEE Transactions on Industrial Electronics*, vol. 65, no. 1, pp. 27-37, 2018.
[33] Y. Zhao and T.A. Lipo, "Space vector PWM control of dual three-phase induction machine using vector space decomposition" *IEEE Transactions on Industry Applications*, vol. 31, no. 5, pp. 1100-1109, 1995.
[34] H. Guzman, M.J. Duran, F. Barrero, B. Bogado and S. Toral, "Speed control of five-phase induction motors with integrated open-phase fault operation using model-based predictive current control techniques", *IEEE Transactions on Industrial Electronics*, vol. 61, no. 9, pp. 4474-4484, 2014.
[35] J. Rodriguez, M.P. Kazmierkowski, J.R. Espinoza, P. Zanchetta, H. Abu-Rub, H.A. Young and C.A. Rojas, "State of the art of finite control set model predictive control in power electronics", *IEEE Transactions on Industrial Informatics*, vol. 9, no. 2, pp. 1003-1016, 2013.
[36] C. Martin, M.R. Arahal, F. Barrero and M.J. Duran, "Five-phase induction motor rotor current observer for finite control set model predictive control of stator current", *IEEE Transactions on Industrial Electronics*, vol. 63, no. 7, pp. 4527-4538, 2016.

Paula Garcia-Entrambasaguas was born in Málaga, Spain, in 1992. She received the University and Master's degrees in Industrial Engineering from the University of Málaga, in 2015 and 2017, respectively.
She is currently working toward the Ph.D. degree in the Electric Power Systems program at University of Málaga, Spain. Her research focuses on multiphase machines and drives and on control methods in pre- and post-fault situations.

Ivan Zoric (S'17) received the BSc and MSc degrees in Electrical Engineering from the University of Belgrade, Serbia in 2010 and 2013, respectively. He joined in June 2014 Liverpool John Moores University, UK, as a PhD student. He completed his PhD in electrical engineering in April 2018 and is since with Dyson. His main research interests include power electronics and advanced machine drives.

Ignacio González Prieto was born in Malaga, Spain, in 1987. He received the Industrial Engineer and M.Sc. degrees in fluid mechanics from the University of Malaga, Malaga, Spain, in 2012 and 2013, ´ respectively, and the Ph.D. degree in electronic engineering from the University of Seville, Sevilla, Spain, in 2016. His research interests include multiphase machines, wind energy systems, and electrical vehicles

Mario J. Duran was born in Bilbao, Spain, in 1975. He received the M.Sc. and Ph.D. degrees in electrical engineering from the University of Malaga, Malaga, in 1999 and 2003, respectively. He is currently a Full Professor in the Department of Electrical Engineering, University of Malaga. His research interests include modeling and ´ control of multiphase drives and renewable energies conversion systems.

Emil Levi (S'89, M'92, SM'99, F'09) received his MSc and the PhD degrees in Electrical Engineering from the University of Belgrade, Yugoslavia in 1986 and 1990, respectively. He joined Liverpool John Moores University, UK in May 1992 and is since September 2000 Professor of Electric Machines and Drives. He served as a Co-Editor-in-Chief of the IEEE Trans. on Industrial Electronics in the 2009-2013 period and is currently Editor-in-Chief of the IET Electric Power Applications and an Editor of the IEEE Trans. on Energy Conversion. He is the recipient of the Cyril Veinott award of the IEEE Power and Energy Society for 2009 and the Best Paper award of the IEEE Trans. on Industrial Electronics for 2008. In 2014 he received the "Outstanding Achievement Award" from the European Power Electronics (EPE) Association.